Indian Journal of Biochemistry & Biophysics
Vol. 59, January 2022, pp. 59-72

Computational evaluation of 2-arylbenzofurans for their potential use against SARS-CoV-2: A DFT, molecular docking, molecular dynamics simulation study

Taner Erdogan*

Department of Chemistry and Chemical Processing Technologies, Kocaeli University, Kocaeli-41140, Turkey

Received 13 March 2021; *revised 15 July 2021*

Natural compounds obtained from various sources have been used in the treatment of many diseases for many years and are very important compounds for drug development studies. They can also be an option to treat COVID-19, which is affecting the whole world and not curable with medication, yet. In this study, two 2-arylbenzofuran derivatives from *Sesbania cannabina* which are newly entered the literature were investigated computationally with the assistance of computational techniques including DFT calculations, molecular docking calculation and molecular dynamics simulations. The study consists of four parts, in the first part of the study DFT calculations were performed on the 2-arylbenzofurans, and geometry optimizations, vibrational analyses, molecular electrostatic potential (MEP) map calculations, frontier molecular orbital (FMO) calculations and Mulliken charge analyses were carried out. In the second part, molecular docking calculations were performed to investigate the interactions between the molecules and two potential target, SARS-CoV-2 main protease (SARS-CoV-2 M^{pro}) and SARS-CoV-2 spike receptor binding domain – human angiotensin converting enzyme 2 complex (SARS-CoV-2 SRBD – hACE2). In the third part, MD simulations were performed on the top-scoring ligand – receptor complexes to investigate the stability of the complex and the interactions between ligands and receptors in more detail. Finally, drug-likeness analyses and ADME (adsorption, desorption, metabolism, excretion) predictions were performed on the investigated compounds. Results showed that investigated natural compounds effectively interacted with the target receptors and gave comparable results to the reference drug molecules.

Keywords: ACE2, COVID-19, Drug-likeness, *In silico* investigation, SARS-CoV-2 main protease

SARS-CoV-2 continues to spread rapidly all over the world since its first appearance in December 2019 and grew into a global pandemic nowadays. Although there are many studies carried out all over the world against SARS-CoV-2, an effective and specific drug treatment has not yet been developed. Studies against COVID-19 can be divided into three groups: (1) vaccine development, (2) drug repurposing and (3) new drug development. Since some drugs on the market are known to be beneficial in the treatment of COVID-19, they are used in the treatment of this disease. However, these drugs are not the drugs developed specifically for COVID-19 and their effectiveness is not at the desired level. For now, although vaccine development studies seem to be the most effective way to develop a treatment in a short time, development of new specific drugs is needed and will be needed in the future, too.

SARS-CoV-2 M^{pro} has an important role in viral replication and transcription, and this makes it an appealing target for the treatment of COVID-19. On the other hand, it is known that SARS-CoV-2 uses its spike receptor binding domain to bind to human angiotensin converting enzyme-2 (hACE2) and enter the human cell. Preventing this interaction between SARS-CoV-2 SRBD and hACE2 could provide an important method for treating the disease, as it could prevent the entrance of the virus into the human cell. In the literature, there are various studies targeted the inhibition of SARS-CoV-2 M^{pro}[1–6] or preventing SARS-CoV-2 SRBD to interact with hACE2[7–9].

In this study, two natural compounds which have recently been added to the literature by Fu *et al*[10]., have been investigated computationally. Fu *et al*. have evaluated the anticancer activities of these natural compounds in their study but to the best of our knowledge these compounds have not yet been studied experimentally or computationally for their antiviral effects against SARS-CoV-2. The structures of these 2-arylbenzofuran derivatives are given in (Fig. 1)[10].

Materials and Methods

DFT Calculations

In this part of the study, geometry optimizations, vibrational analyses, MEP map calculations, FMO

*Correspondence:
E-mail: erdogantaner@outlook.com.tr

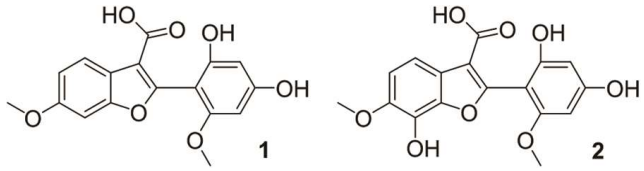

Fig. 1 — Molecular structures of 2-arylbenzofurans

calculations and Mulliken charge analyses were carried out. All calculations in this part were performed in both gas and solution phasewith the use of Becke three-parameter hybrid functional combined with Lee-Yang-Parr correlation functional (B3LYP) and Austin-Frisch-Petersson functional with dispersion method (APF-D). In the calculations performed in solution phase, IEFPCM (Polarizable Continuum Model using the integral equation formalism variant) solvation model was used, and water was selected as solvent. All the calculations were performed with the use 6-311+G(2d,p) basis set. Gaussian 09 Rev.D01[11], GaussView 5[12], VeraChemV conf[13] software packages were used in the calculations.

Molecular Docking Calculations

In molecular docking calculations, the structures of SARS-CoV-2 $M^{pro}$and SARS-CoV-2 SRBD – hACE2 were obtained from RCSB Protein Data Bank (PDB ID: 5r80 and 6lzg)[14–16]. The 3D structures of 2-arylbenzofurans were obtained from DFT calculations. In molecular docking calculations, AutoDock Tools[17]and AutoDock Vina[18] program packages were used and Discovery Studio Visualizer[19] was used in the representation of the docking results. Water and ligand molecules were removed, hydrogens and Gasteiger charges were added to prepare the receptors for docking. Lamarckian genetic algorithm was used in the docking procedure. Gridbox size was set to 20 × 25 × 20 $Å^3$ and 20 × 20 × 20 $Å^3$ for SARS-CoV-2 M^{pro} and SARS-CoV-2 SRBD – hACE2, respectively, and grid spacing was set to 1 Å in all cases. After each docking calculation, nine docking poses having highest binding scores were obtained.

Molecular Dynamics Simulations

MD simulation studies on top-scoring ligand – receptor complexes followed the molecular docking calculations to investigate the interactions in more detail and to investigate the stability of the complexes. MD simulations were performed for 30 ns. In MD simulations, GROMACS 2020[20] program package was used. Ligand topologies were obtained from Acpype Server[21] and topologies of the receptors were obtained with the use of AMBER[22] force field and

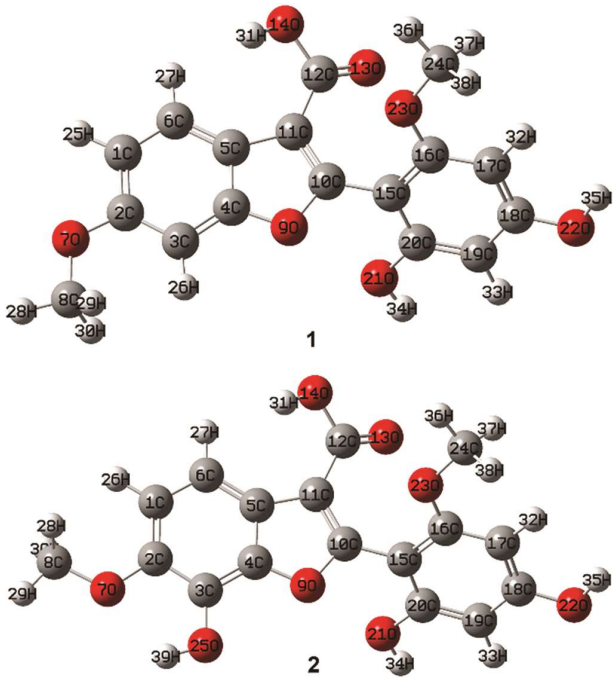

Fig. 2 — Geometry optimized structures of the investigated compounds

TIP3P water model. First, in each case, system was neutralized, and energy minimization procedure was run by employing steepest descent minimization algorithm. NVT and NPT ensemble equilibrations were performed for 200 ps. MD simulations were performed in a dodecahedron simulation box at 1 bar and 300 K reference pressure and temperature.

Drug-likeness Analyses and ADME Predictions

Drug-likeness analyses and ADME predictions were performed *via* Swiss ADME[23]web server and some important parameters such as physicochemical properties, lipophilicity and water solubility were predicted. In this part, Lipinski[24], Ghose[25], Veber[26], Egan[27] and Muegge[28] filters were used to perform drug-likeness analysis on the investigated compounds.

Results and Discussion

DFT Calculations

In this part, a conformer search was carried out prior to geometry optimizations in order to assure that global minimum was obtained for each structure. Additionally, frequency calculations followed the geometry optimizations to confirm that each optimized geometry corresponds to a global minimum. Geometry optimized structures of the investigated compounds which were obtained in gas phase with the use of B3LYP method and 6-311+G(2d,p) basis set are given in (Fig. 2). In Figure 3, calculated

infrared spectra of the investigated compounds obtained at the same level of theory are given.

MEP maps give information about the electron rich and electron deficient parts of a given molecule. These electron rich and electron deficient centers play important role in the interactions between investigated compounds and receptors. MEP maps of the investigated compounds are given in (Fig. 4). Results showed that negative charge was predominantly on the oxygen atoms, while hydroxyl group hydrogens carried positive charge. The results also showed that the method used in the calculations and the phase in which the calculations were performed (gas or solution phase) affect the charge distribution in MEP maps. It was observed that the charge ranges obtained from the calculations performed in solution phase are wider than the ranges obtained from the calculations performed in gas phase. It was also seen that the charge ranges obtained with the use of APF-Dare wider than the ranges obtained with the use of B3LYP.

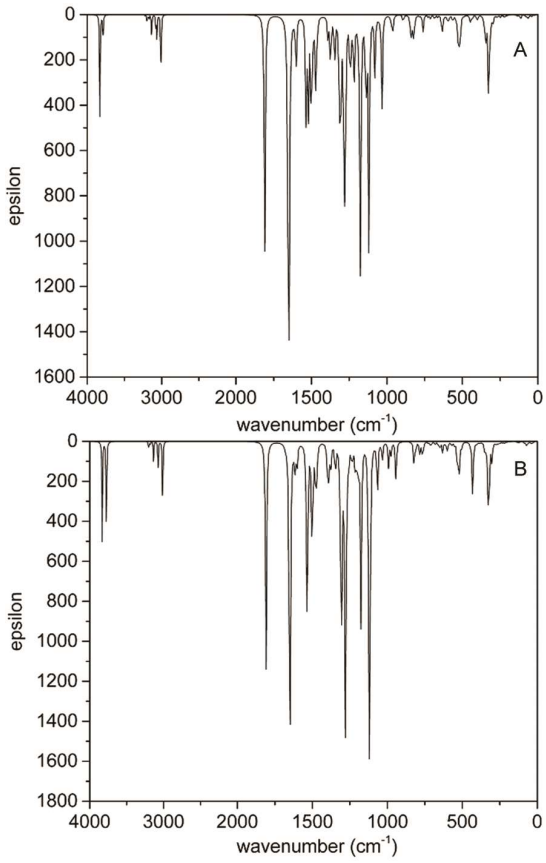

Fig. 3 — Calculated infrared spectra of the investigated compounds (A) compound 1; and (B) compound 2

HOMO and LUMOs of a given molecule are used to estimate how this molecule interacts with other compounds. HOMO and LUMOs of the investigated compounds and the energies obtained with the use of different methods are given in (Fig. 5). Results showed that in gas phase, HOMO-LUMO gaps of compound 2 were found to be larger than those of compound 1. In contrast to gas phase, results obtained from the calculations performed in water showed that HOMO-LUMO gaps of compound 1 were found to be larger than those of compound 2. FMO analyses indicated that delocalization is occurred over all atoms except methyl groups for both molecules. Additionally, relatively large HOMO-LUMO gaps indicate that both molecules have quite stable structures.

Calculated Mulliken charges of the investigated compounds with the use of B3LYP and APF-D in gas phase and solution phase are given in (Table 1). In both cases 6-311+G(2d,p) basis set was used.

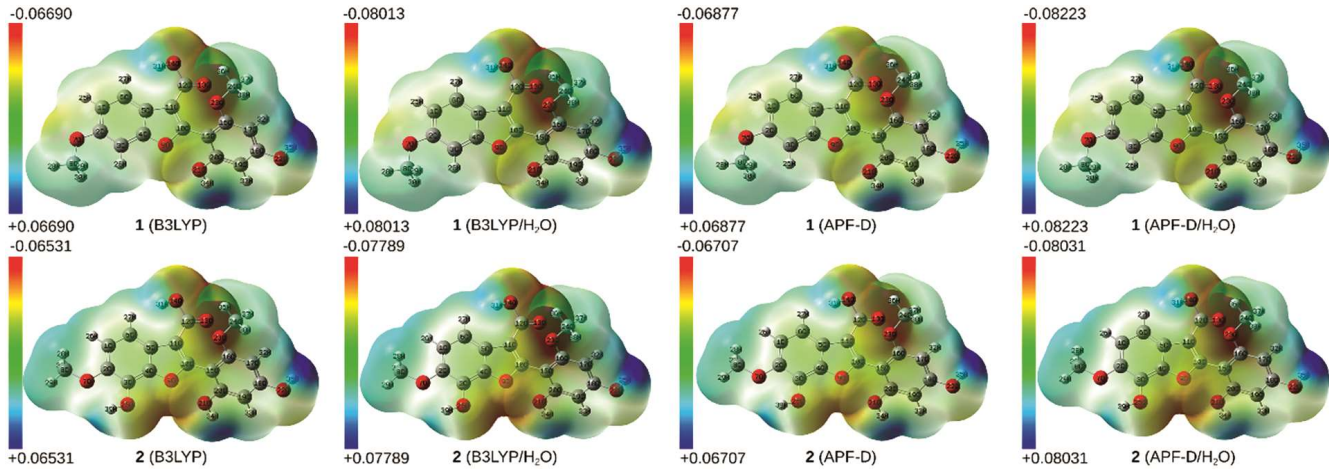

Fig. 4 — MEP maps of the investigated compounds

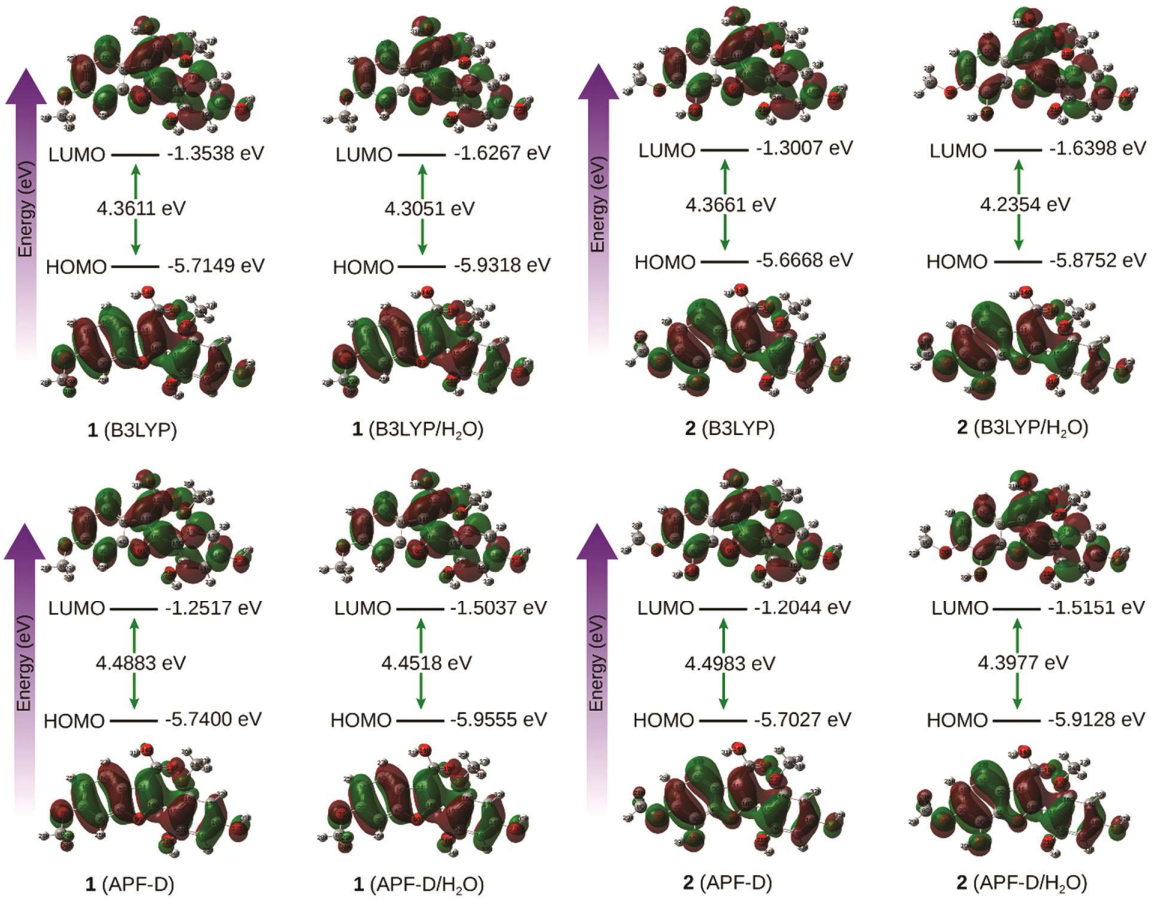

Fig. 5 — FMOs of the investigated compounds

Mulliken atomic charges of a given molecule significantly influence some important parameters such as dipole moment, polarizability, and electronic structure. For both compounds, all hydrogen atoms have a positive charge while all oxygen atoms have a negative charge. On the other hand, the Mulliken charges of carbon atoms highly influenced by their environment and have both positive and negative charges.

Molecular Docking Calculations

Molecular docking calculations were performed to obtain top-scoring docking poses for compounds 1 and 2. Additionally, to make a comparison, calculations were repeated for remdesivir, lopinavir, favipiravir and hydroxychloroquine which are the drugs currently under investigation for their potential use against COVID-19. Especially remdesivir is widely used because of being an FDA-approved drug for the treatment of COVID-19. 3D structures of remdesivir, favipiravir and hydroxychloroquine were obtained from PubChem Database[29] and the structure of lopinavir was obtained from Zinc Database[30]. Results for SARS-CoV-2-SRBD – hACE2 showed that, investigated 2-arylbenzofurans have higher binding score than all other compounds. On the other hand, for SARS-CoV-2 M^{pro}, the binding scores of 2-arylbenzofurans are higher than those of favipiravir and hydroxychloroquine and comparable to the binding scores of lopinavir and remdesivir (Table 2).

Molecular Dynamics Simulations

After performing molecular docking calculations, 30 ns molecular dynamics simulations were performed for each top-scoring ligand-receptor complex to investigate the stability and the ligand-receptor interactions in more detail.

In Figure 6, the superimposed structures of SARS-CoV-2 M^{pro} – 1 complex extracted every 5 ns of the simulation are given. 2D representations of these interactions are given in (Fig. 7). Results showed that ligand remained in the receptor binding pocket throughout the entire simulation.

Table 1 — Mulliken atomic charges of compounds 1 and 2

	Mulliken Charges					Mulliken Charges			
Comp. 1	B3LYP	B3LYP/H_2O	APF-D	APF-D/H_2O	Comp. 2	B3LYP	B3LYP/H_2O	APF-D	APF-D/H_2O
1C	−0.286	−0.345	−0.427	−0.474	1C	−0.061	−0.055	0.054	0.078
2C	0.382	0.391	0.347	0.345	2C	0.319	0.306	0.255	0.223
3C	−0.481	−0.425	−0.482	−0.437	3C	−0.242	−0.257	−0.424	−0.431
4C	0.249	0.254	0.158	0.148	4C	0.185	0.169	−0.010	−0.030
5C	0.710	0.696	0.927	0.928	5C	0.721	0.704	0.920	0.925
6C	−0.254	−0.276	−0.346	−0.370	6C	−0.754	−0.736	−0.897	−0.930
7O	−0.454	−0.486	−0.388	−0.418	7O	−0.570	−0.575	−0.502	−0.506
8C	−0.158	−0.168	−0.252	−0.266	8C	−0.148	−0.165	−0.245	−0.264
9O	−0.400	−0.416	−0.353	−0.371	9O	−0.410	−0.438	−0.369	−0.400
10C	0.042	−0.003	0.083	−0.039	10C	0.296	0.269	0.429	0.311
11C	0.402	0.313	0.636	0.549	11C	0.474	0.393	0.764	0.708
12C	0.063	0.208	−0.158	0.017	12C	0.201	0.367	−0.048	0.159
13O	−0.419	−0.508	−0.405	−0.487	13O	−0.414	−0.501	−0.402	−0.481
14O	−0.321	−0.364	−0.292	−0.336	14O	−0.326	−0.368	−0.297	−0.342
15C	0.288	0.224	0.346	0.245	15C	0.328	0.241	0.442	0.316
16C	0.456	0.428	0.231	0.361	16C	0.463	0.432	0.210	0.351
17C	−0.499	−0.440	−0.448	−0.426	17C	−0.516	−0.450	−0.476	−0.442
18C	0.040	0.056	0.062	0.005	18C	0.057	0.075	0.096	0.031
19C	−0.286	−0.276	−0.367	−0.333	19C	−0.327	−0.309	−0.438	−0.390
20C	0.322	0.298	0.262	0.249	20C	0.370	0.351	0.337	0.301
21O	−0.460	−0.505	−0.454	−0.500	21O	−0.455	−0.504	−0.448	−0.498
22O	−0.429	−0.467	−0.413	−0.448	22O	−0.429	−0.466	−0.413	−0.447
23O	−0.442	−0.466	−0.351	−0.379	23O	−0.440	−0.464	−0.345	−0.376
24C	−0.157	−0.168	−0.267	−0.260	24C	−0.157	−0.167	−0.272	−0.263
25H	0.094	0.112	0.114	0.133	25O	−0.478	−0.527	−0.477	−0.522
26H	0.100	0.128	0.119	0.147	26H	0.088	0.120	0.109	0.141
27H	0.100	0.120	0.124	0.142	27H	0.098	0.117	0.120	0.140
28H	0.139	0.151	0.160	0.172	28H	0.139	0.153	0.162	0.176
29H	0.136	0.152	0.162	0.177	29H	0.142	0.155	0.161	0.175
30H	0.138	0.152	0.162	0.177	30H	0.141	0.154	0.164	0.177
31H	0.245	0.289	0.250	0.292	31H	0.245	0.290	0.249	0.293
32H	0.071	0.117	0.090	0.138	32H	0.071	0.117	0.090	0.138
33H	0.081	0.113	0.100	0.134	33H	0.081	0.113	0.101	0.135
34H	0.288	0.329	0.292	0.333	34H	0.290	0.330	0.294	0.333
35H	0.273	0.313	0.280	0.319	35H	0.273	0.313	0.279	0.319
36H	0.144	0.156	0.165	0.176	36H	0.144	0.156	0.164	0.176
37H	0.153	0.159	0.188	0.186	37H	0.153	0.159	0.188	0.186
38H	0.130	0.153	0.147	0.173	38H	0.131	0.153	0.147	0.173
					39H	0.318	0.345	0.327	0.353

Table 2 — Binding scores of the investigated compounds.

Compound	6LZG[1]	5R80[2]
1	−7.5	−7.6
2	−7.4	−7.0
Remdesivir	−6.9	−7.9
Lopinavir	−6.8	−8.2
Favipiravir	−6.8	−5.1
Hydroxychloroquine	−5.9	−6.3

[1]SARS-CoV-2 SRBD – hACE2
[2]SARS-CoV-2 M^{pro}

Results for SARS-CoV-2 M^{pro} – 1 complex showed that, in most of the simulation time, MET49, PRO168, MET165, GLN189, HIS41, THR190 and ARG188 took part in the interactions between ligand and receptor.

Superimposed structures of the SARS-CoV-2 M^{pro} – 2 complex extracted every 5 ns of the simulation are given in (Fig. 8) and 2D representations of these interactions are given in (Fig. 9). Results showed that ligand remained in the receptor binding pocket throughout the entire simulation.

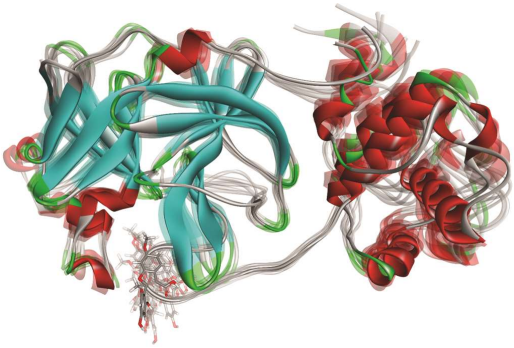

Fig. 6 — Superimposed structures of SARS-CoV-2 M^{pro}– 1 complex extracted every 5 ns of the simulation

Results showed that, when compared to SARS-CoV-2 M^{pro} – 1 complex, for SARS-CoV-2 M^{pro} – 2 complex there were considerable differences in the interactions between ligand and receptor. In this complex, in most of the simulation time, CYS145, THR26, SER46 and THR25 took part in the interactions between ligand and receptor. When considered together with the binding score, it can be concluded that the interactions in this complex are lower than those in the SARS-CoV-2 M^{pro} – 1 complex.

Superimposed structures of SARS-CoV-2 SRBD-hACE2 – 1 complex extracted every 5 ns of the

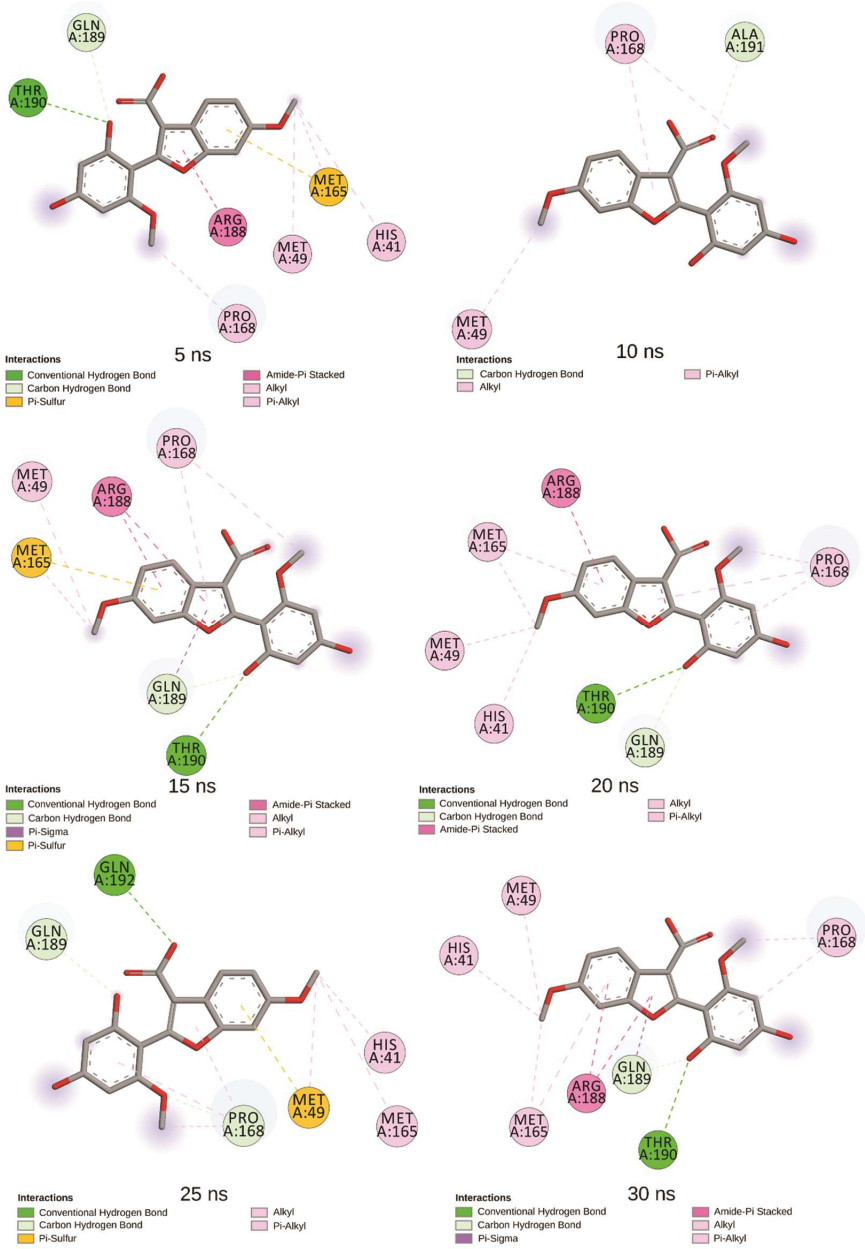

Fig. 7 — 2D representations of the ligand – receptor interactions in SARS-CoV-2 M^{pro}– 1 complex

simulation are given in (Fig. 10) and 2D representations of these interactions are given in (Fig. 11). Results showed that ligand remained in the receptor binding pocket in the interface between SARS-CoV-2 SRBD and hACE2 throughout the entire simulation.

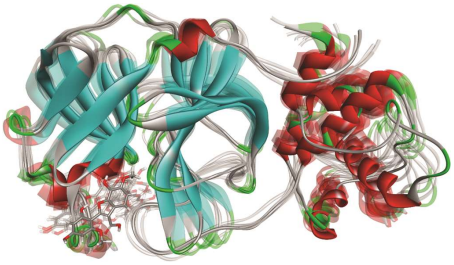

Fig. 8 — Superimposed structures of SARS-CoV-2 M^{pro} – 2 complex extracted every 5 ns of the simulation

Results for SARS-CoV-2 SRBD-hACE2 – 1 complex showed that, throughout almost the entire simulation period, PRO389, ASP30 and HIS34 took part in the interactions between ligand and receptor. Additionally, LEU29, GLN96, LYS417, LYS26, ASN33, GLN388,

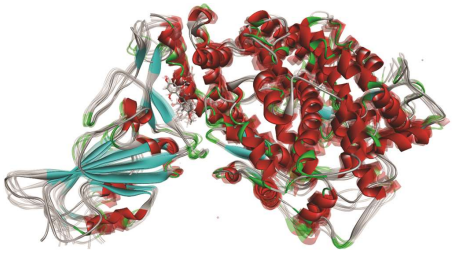

Fig. 10 — Superimposed structures of SARS-CoV-2 SRBD-hACE2 – 1 complex extracted every 5 ns of the simulation

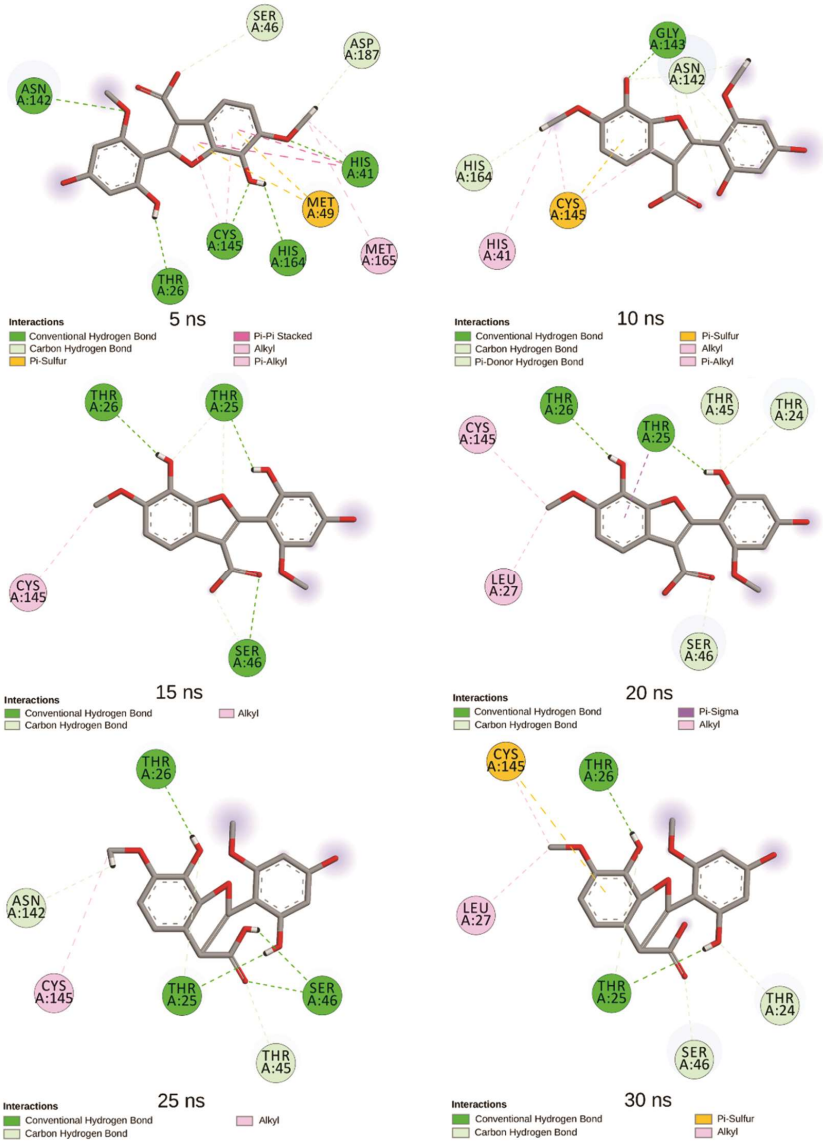

Fig. 9 — 2D representations of the ligand – receptor interactions in SARS-CoV-2 M^{pro}– 2 complex

ARG393, ALA386, ALA387, ARG403 and TYR453 took part in the stabilization of the complex.

Finally, superimposed structures of SARS-CoV-2 SRBD-hACE2 – 2 complex extracted every 5 ns of the simulation are given in (Fig. 12 and 2D) representations of these interactions are given in (Fig. 13). Results showed that ligand remained in the receptor binding pocket in the interface between SARS-CoV-2 SRBD and hACE2 throughout the entire simulation.

Results showed that, when compared to SARS-CoV-2 SRBD-hACE2 – 1 complex, for SARS-CoV-2 SRBD-hACE2 – 2 complex there were some differences in the interactions between ligand and receptor. In this complex, in most of the simulation time, HIS34, GLU35, SER494, TYR505, ARG403, GLU406 and ASN33 took part in the interactions between ligand and receptor. Additionally, GLU37, LYS353, ARG393, ALA387, PRO389, TYR495, ASP38 and GLN388 participated in the interactions.

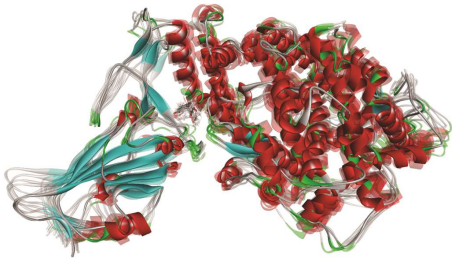

Fig. 12 — Superimposed structures of SARS-CoV-2 SRBD-hACE2 – 2 complex extracted every 5 ns of the simulation

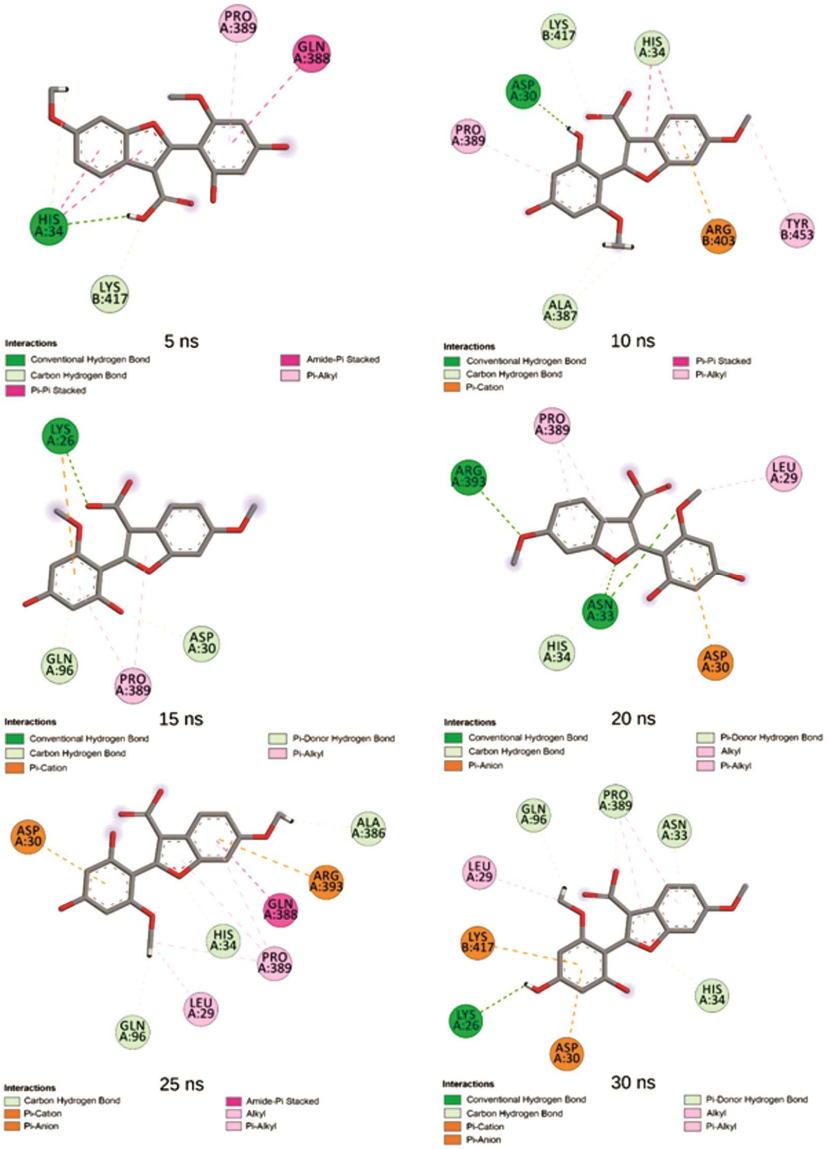

Fig. 11 — 2D representations of the ligand – receptor interactions in SARS-CoV-2 SRBD-hACE2 – 1 complex

The interactions in the structures of all complexes belong to 30th ns of the simulation are shown in (Fig. 14).

Root mean square deviation (RMSD) and radius of gyration (RG) are often used to determine the stability of proteins. RMSDs of proteins compared to their initial positions in all four ligand-receptor complexes are given in (Fig. 15). Average RMSD values of proteins and standard deviations were found to be 0.2535 (0.1306), 0.2491 (0.1321), 0.2548 (0.1297) and 0.2954 (0.1346) nm for SARS-CoV-2 M^{pro}– 1, SARS-CoV-2 M^{pro}– 2, SARS-CoV-2 SRBD-hACE2 – 1 and SARS-CoV-2 SRBD-hACE2 – 2 complexes, respectively.

In the study, RMSDs of ligands compared to the position of the receptors were monitored for each complex to investigate how well the binding poses were preserved during the MD simulation. Obtained results are given in (Fig. 16).

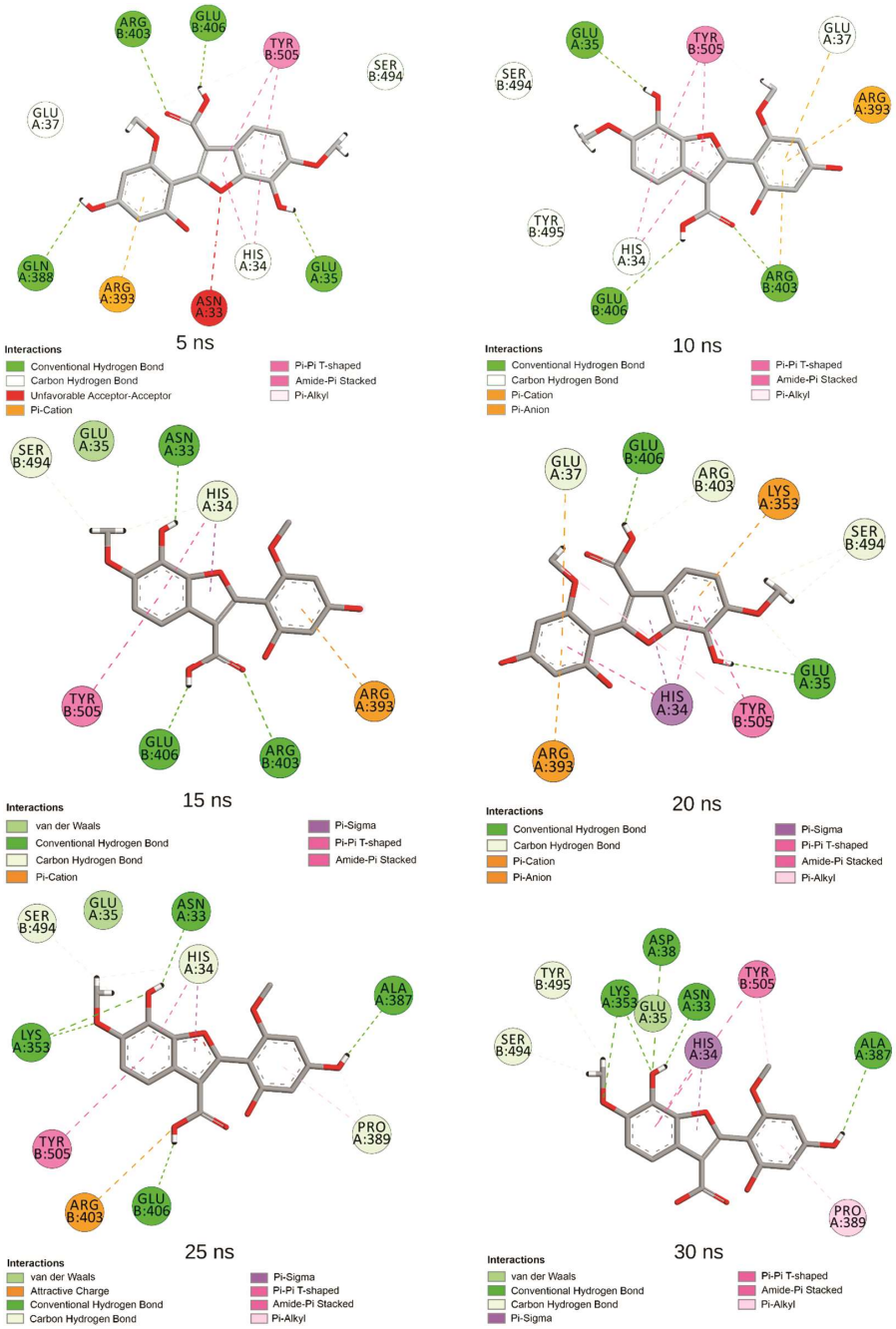

Fig. 13 — 2D representations of the ligand – receptor interactions in SARS-CoV-2 SRBD-hACE2 – 2 complex

Results showed that there was no considerable change in the relative position of the ligand in SARS-CoV-2 M^{pro}– 1 and SARS-CoV-2 SRBD-hACE2 – 2 complexes (Fig. 16A-D). For SARS-CoV-2 M^{pro}– 2 and SARS-CoV-2 SRBD-hACE2 – 1 complexes, it was found that the position of the ligand reached its equilibrium position about 15th ns and after this time there was no considerable change in the relative position of the ligand.

Radius of gyration is another parameter to estimate the stability of a given protein. RG of the proteins in all four complexes were monitored during the MD simulation and are given in (Fig. 17).

Average RG values of proteins and standard deviations were found to be 2.2316 (0.0138), 2.2331 (0.0141), 3.1341 (0.0204)and 3.1296 (0.0205) nm for SARS-CoV-2 M^{pro} – 1, SARS-CoV-2 M^{pro} – 2, SARS-CoV-2 SRBD-hACE2 – 1 and SARS-CoV-2 SRBD-

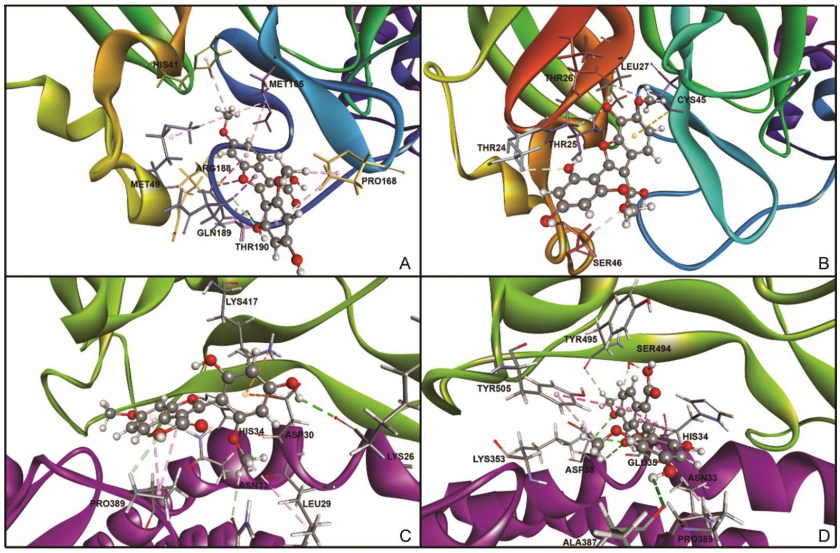

Fig. 14 — The interactions in the structures of the complexes belong to 30th ns of the MD simulation (A) SARS-CoV-2 M^{pro}– 1; (B) SARS-CoV-2 M^{pro}– 2; (C) SARS-CoV-2 SRBD-hACE2 – 1; and (D) SARS-CoV-2 SRBD-hACE2 – 2

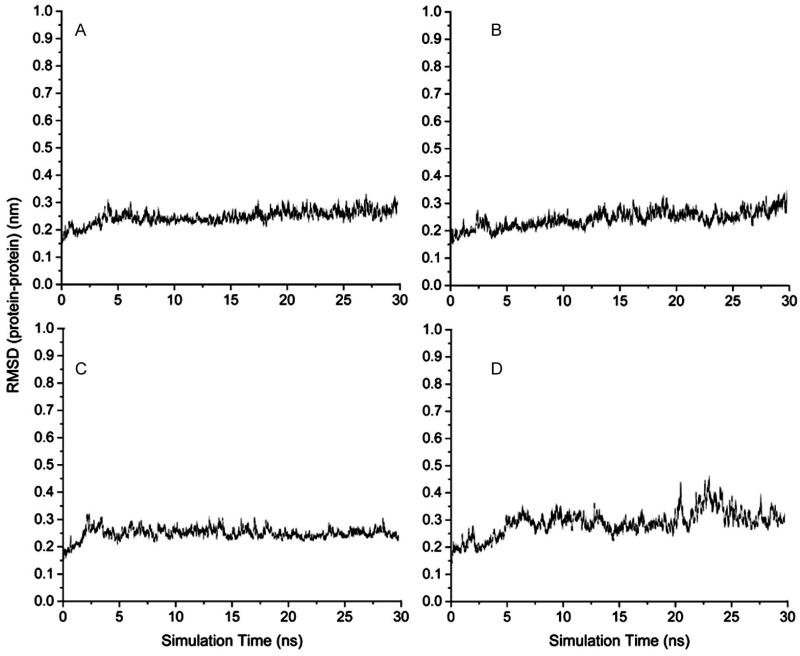

Fig. 15 — RMSDs of proteins compared to their initial positions (A) SARS-CoV-2 M^{pro}– 1; (B) SARS-CoV-2 M^{pro}– 2; (C) SARS-CoV-2 SRBD-hACE2 – 1; and (D) SARS-CoV-2 SRBD-hACE2 – 2

hACE2 – 2 complexes, respectively. Results showed that there was no considerable change in the radius of gyration of the proteins in all of the complexes.

Drug-likeness and ADME Predictions

In the study, in addition to DFT calculations, molecular docking calculations and molecular dynamics simulations, drug-likeness analyses and ADME predictions were performed via Swiss ADME web server[23]. Drug-likeness and ADME prediction results are given in (Tables 3 & 4).

Results showed that both molecules have no more than 10 hydrogen bond acceptors and 5 hydrogen bond donors which means both molecules obey the Lipinski rule. Molecular weights do not exceed the

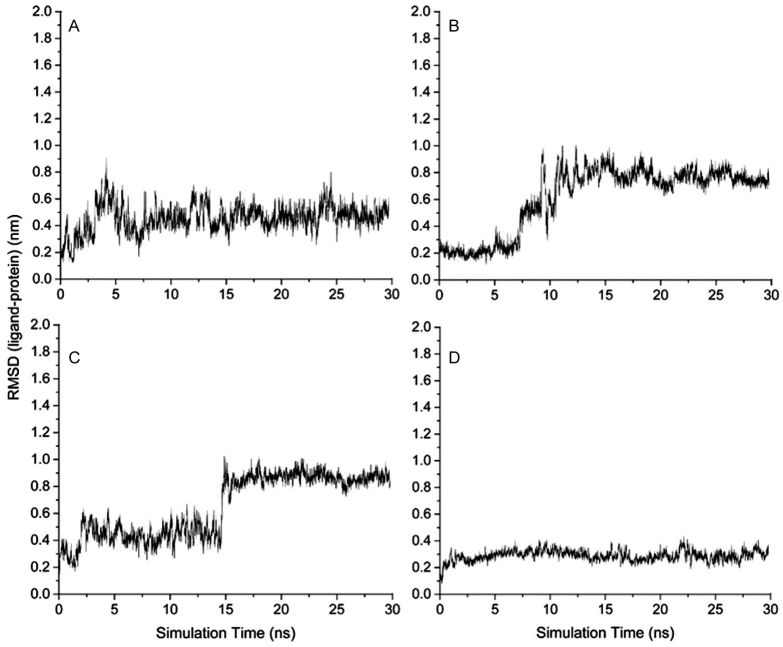

Fig. 16 — RMSDs of ligands compared to the positions of the receptors (A) SARS-CoV-2 M^{pro}– 1; (B) SARS-CoV-2 M^{pro}– 2; (C) SARS-CoV-2 SRBD-hACE2 – 1; and (D) SARS-CoV-2 SRBD-hACE2 – 2

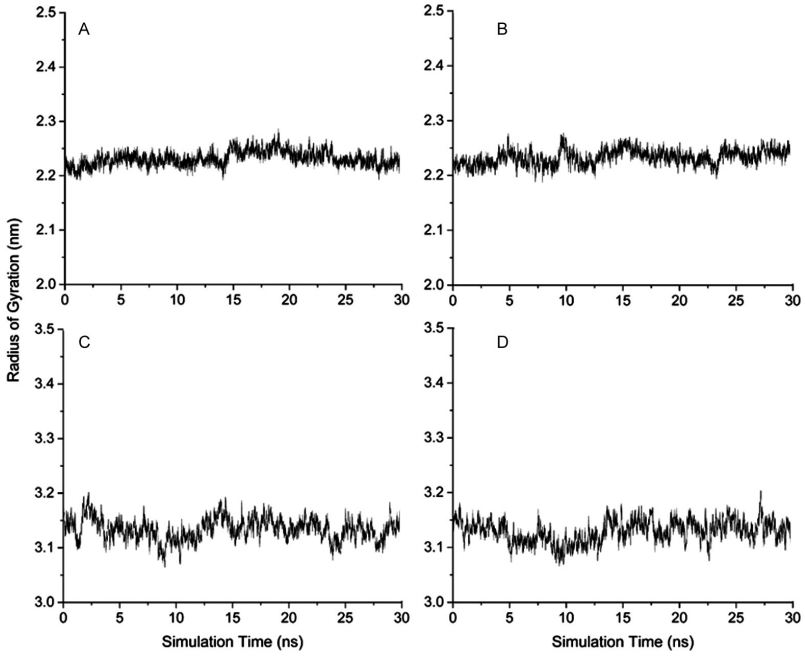

Fig. 17 — Change in the RG of protein during the MD simulation (A) SARS-CoV-2 M^{pro} – 1; (B) SARS-CoV-2 M^{pro} – 2; (C) SARS-CoV-2 SRBD-hACE2 – 1; and (D) SARS-CoV-2 SRBD-hACE2 – 2

Table 3 — Results of ADME analyses of the investigated compounds

Compound	1	2
Physicochemical Properties		
Number of H-Bond Acceptors	7	8
Number of H-Bond Donors	3	4
Molecular Weight (g/mol)	330.3	346.3
Number of heavy atoms	24	25
Number of aromatic heavy atoms	15	15
Fraction C sp^3	0.12	0.12
Number of rotatable bonds	4	4
Molar refractivity	85.64	87.66
TPSA ($Å^2$)	109.36	129.59
Lipophilicity		
iLOGP	2.26	1.95
XLOGP3	2.75	2.39
WLOGP	3.23	2.93
MLOGP	0.78	0.26
SILICOS-IT	2.45	1.97
Consensus $logP_{o/w}$	2.29	1.90
Water Solubility		
ESOL	S	S
ALI	MS	MS
SILICOS-IT	MS	S
Pharmacokinetics		
GI Absorption	High	High
BBB Permeation	No	No
Skin permeation, $logK_p$ (cm/s)	−6.36	−6.72

TPSA: Topological Polar Surface Area, GI: Gastrointestinal, BBB: Blood Brain Barrier, MS: Moderately soluble, S: Soluble, VS: Very soluble

limits suggested by Lipinski and Ghose rules. Number of rotatable bonds was found to be 4 for both molecules and met the requirements of Veber and Muegge rules. Fraction C sp^3 value was found to be 0.12 for both molecules. Increasing fraction C sp^3 values correspond to higher degrees of saturation and it is proposed that increasing degrees of saturation increases the clinical success rate of a molecule[31,32].

Molar refractivities of the molecules 1 and 2 were found to be 85.64 and 87.66, respectively. Since the Ghose rule states that the molar refractivity should be between 40-130, both molecules fulfill this rule. In prediction of the drug-likeness of a given molecule, topological polar surface area (TPSA) is also used[33]. TPSA values of the compounds were found to be 109.36 and 129.59 $Å^2$, respectively, and met the requirements of Veber rule. As is known, Veber rule

Table 4 — Results of drug-likeness and medicinal chemistry analyses

Compound	1	2
Drug-likeness		
Lipinksi	Yes	Yes
Ghose	Yes	Yes
Veber	Yes	Yes
Egan	Yes	Yes
Muegge	Yes	Yes
ABS	0.56	0.56
Medicinal Chemistry		
PAINS	0 alert	0 alert
Brenk	0 alert	0 alert
Leadlikeness	Yes	Yes
SAS	3.32	3.44

ABS: Abbott Bioavailabilty Score, PAINS: Pan Assay Interference Structures, SAS: Synthetic Accessibility Score

stated that the TPSA of a given molecule should not be greater than 140 $Å^2$. The average partition coefficient[34–40] of the molecules 1 and 2 were found to be 2.29 and 1.90, respectively. According to ESOL[41] and ALI[42], water solubilities of molecules 1 and 2 were predicted to be soluble and moderately soluble, respectively. On the other hand, SILICOS-IT[40] predicted that the water solubility of molecules 1 and 2 are moderately soluble and soluble, respectively. Gastrointestinal absorptions of the molecules were predicted to be high, but it was predicted that molecules cannot penetrate blood-brain barrier.

In the study it was found that both molecules obey Lipinski, Ghose, Veber, Egan and Muegge rules, and bioavailability scores[43] were estimated to be 0.56 for both molecules. Additionally, no alert was observed for PAINS[44], Brenk[45] and leadlikeness[46] analyses, and synthetic accessibility scores of molecules 1 and 2 were found to be 3.32 and 3.44, respectively.

Conclusion

In the study, DFT calculations, molecular docking calculations, MD simulation studies, drug-likeness analyses and ADME predictions have been performed on two newly introduced 2-arylbenzofuran derivatives obtained from *Sesbania cannabina* by Fu *et al.*[9], to investigate them computationally for their potential use against SARS-CoV-2. In DFT calculations, four different methods (B3LYP/6-311+G(2d,p) in gas phase, B3LYP/6-311+G(2d,p) in solution phase, APF-D/6-311+G(2d,p) in gas phase and APF-D/6-311+G(2d,p) in solution phase) were used for each compound and the results were compared. In molecular docking and MD simulation studies, two potential targets, SARS-CoV-2 M^{pro} and SARS-CoV-2

SRBD – hACE2 complexes, suggested for the treatment of COVID-19 were selected. Results showed that the compounds were effectively bound to the active sites of the investigated receptors and remained in the binding pocket throughout the entire MD simulation. Additionally, in drug-likeness and ADME analyses, no violation was observed for the investigated 2-arylbenzofuran derivatives. In the study, it was concluded that the investigated compounds can be promising structures for further studies on COVID-19 treatment.

Acknowledgement

The computational studies reported in this paper were partially performed at TÜBİTAK ULAKBİM, High Performance and Grid Computing Center (TRUBA resources) and Kocaeli University.

Conflict of interest

All authors declare no conflict of interest.

References

1 Sepay N, Sekar A, Halder UC, Alarifi A & Afzal M, Anti-COVID-19 terpenoid from marine sources: A docking, admet and molecular dynamics study. *J Mol Struct*, 1228 (2021) 129433.

2 Holanda VN, Lima EM de A, Silva WV da, Maia RT, Medeiros R de L, Ghosh A, Lima VL de M & Figueiredo RCBQ de, Identification of 1,2,3-triazole-phthalimide derivatives as potential drugs against COVID-19: a virtual screening, docking and molecular dynamic study. *J Biomol Struct Dyn*, (2021) 1.

3 Singh E, Khan RJ, Jha RK, Amera GM, Jain M, Singh RP, Muthukumaran J & Singh AK, A comprehensive review on promising anti-viral therapeutic candidates identified against main protease from SARS-CoV-2 through various computational methods. *J Genet Eng Biotechnol*, 18 (2020) 1.

4 Escorcia AM, van Rijn JPM, Cheng G-J, Schrepfer P, Brück TB & Thiel W, Molecular dynamics study of taxadiene synthase catalysis. *J Comput Chem*, 39 (2018) 1215.

5 Erdogan T, DFT, molecular docking and molecular dynamics simulation studies on some newly introduced natural products for their potential use against SARS-CoV-2. *J Mol Struct*, 1242 (2021) 130733.

6 Mishra AK & Tewari SP, *In silico* screening of some naturally occurring bioactive compounds predicts potential inhibitors against SARS-COV-2 (COVID-19) protease. *Indian J Biochem Biophys*, 5 (2021) 416.

7 Muhseen ZT, Hameed AR, Al-Hasani HMH, Tahir ul Qamar M & Li G, Promising terpenes as SARS-CoV-2 spike receptor-binding domain (RBD) attachment inhibitors to the human ACE2 receptor: Integrated computational approach. *J Mol Liq*, 320 (2020) 114493.

8 Parida PK, Paul D & Chakravorty D, The natural way forward: Molecular dynamics simulation analysis of phytochemicals from Indian medicinal plants as potential inhibitors of SARS-CoV-2 targets. *Phyther Res*, 34 (2020) 3420.

9 Prasanth DSNBK, Murahari M, Chandramohan V, Panda SP, Atmakuri LR & Guntupalli C, *In silico* identification of potential inhibitors from Cinnamon against main protease and spike glycoprotein of SARS CoV-2. *J Biomol Struct Dyn*, (2020) 1.

10 Fu XJ, Yi JL, Yang JY, Lin XQ, Huang WH & Zhou XM, Bioactive 2-arylbenzofurans derivatives from Sesbania cannabina. *Phytochem Lett*, 41 (2021) 106.

11 Frisch MJ, Trucks GW, Schlegel HB, Scuseria GE, Robb MA, Cheeseman JR, Scalmani G, Barone V, Mennucci B, Petersson GA, Nakatsuji H, Caricato M, Li X, Hratchian HP, Izmaylov AF, Bloino J, Zheng G, Sonnenberg JL, Hada M, Ehara M, Toyota K, Fukuda R, Hasegawa J, Ishida M, Nakajima T, Honda Y, Kitao O, Nakai H, Vreven T, Montgomery J. A. J, Peralta JE, Ogliaro F, Bearpark M, Heyd JJ, Brothers E, Kudin KN, Staroverov VN, Keith T, Kobayashi R, Normand J, Raghavachari K, Rendell A, Burant JC, Iyengar SS, Tomasi J, Cossi M, Rega N, Millam JM, Klene M, Knox JE, Cross JB, Bakken V, Adamo C, Jaramillo J, Gomperts R, Stratmann RE, Yazyev O, Austin AJ, Cammi R, Pomelli C, Ochterski JW, Martin RL, Morokuma K, Zakrzewski VG, Voth GA, Salvador P, Dannenberg JJ, Dapprich S, Daniels AD, Farkas O, Foresman JB, Ortiz J V, Cioslowski J & Fox DJ, Gaussian 09, (2013).

12 Dennington R, Keith T & Millam J, GaussView, Version 5. (2009).

13 Chang C-E & Gilson MK, Tork: Conformational analysis method for molecules and complexes. *J Comput Chem*, 24 (2003) 1987.

14 RCSB PDB, https://www.rcsb.org/

15 Douangamath A, Fearon D, Gehrtz P, Krojer T, Lukacik P, Owen CD, Resnick E, Strain-Damerell C, Aimon A, Ábrányi-Balogh P, Brandão-Neto J, Carbery A, Davison G, Dias A, Downes TD, Dunnett L, Fairhead M, Firth JD, Jones SP, Keeley A, Keserü GM, Klein HF, Martin MP, Noble MEM, O'Brien P, Powell A, Reddi RN, Skyner R, Snee M, Waring MJ, Wild C, London N, von Delft F & Walsh MA, Crystallographic and electrophilic fragment screening of the SARS-CoV-2 main protease. *Nat Commun*, 11 (2020) 5047.

16 Wang Q, Zhang Y, Wu L, Niu S, Song C, Zhang Z, Lu G, Qiao C, Hu Y, Yuen KY, Wang Q, Zhou H, Yan J & Qi J, Structural and functional basis of SARS-CoV-2 entry by using human ACE2.*Cell*, 181 (2020) 894.

17 Morris GM, Huey R, Lindstrom W, Sanner MF, Belew RK, Goodsell DS & Olson AJ, AutoDock4 and AutoDockTools4: Automated docking with selective receptor flexibility. *J Comput Chem*, 30 (2009) 2785.

18 Trott O & Olson AJ, AutoDock Vina: Improving the speed and accuracy of docking with a new scoring function, efficient optimization, and multithreading. *J Comput Chem*, 31 (2010) 455.

19 BIOVIA DS, Discovery Studio Visualizer, v20.1.0.19295. (2016).

20 Lindahl E, Abraham MJ, Hess B & van der Spoel D, GROMACS 2020 Source code, (2020).

21 Sousa Da Silva AW & Vranken WF, ACPYPE - AnteChamber PYthon Parser interfacE. *BMC Res Notes*, 5 (2012) 367.

22 Ponder JW & Case DA, Force fields for protein simulations. *Adv Protein Chem*, 66 (2003) 27.

23 Daina A, Michielin O & Zoete V, Swiss ADME: A free web tool to evaluate pharmacokinetics, drug-likeness and medicinal chemistry friendliness of small molecules. *Sci Rep*, 7 (2017) 1.

24 Lipinski CA, Lombardo F, Dominy BW & Feeney PJ, Experimental and computational approaches to estimate solubility and permeability in drug discovery and development settings. *Adv Drug Deliv Rev*, 46 (2001) 3.

25 Ghose AK, Viswanadhan VN & Wendoloski JJ, A knowledge-based approach in designing combinatorial or medicinal chemistry libraries for drug discovery. 1. A qualitative and quantitative characterization of known drug databases. *J Comb Chem*, 1 (1999) 55.

26 Veber DF, Johnson SR, Cheng HY, Smith BR, Ward KW & Kopple KD, Molecular properties that influence the oral bioavailability of drug candidates. *J Med Chem*, 45 (2002) 2615.

27 Egan WJ, Merz KM & Baldwin JJ, Prediction of drug absorption using multivariate statistics. *J Med Chem*, 43 (2000) 3867.

28 Muegge I, Heald SL & Brittelli D, Simple selection criteria for drug-like chemical matter. *J Med Chem*, 44 (2001) 1841.

29 Kim S, Chen J, Cheng T, Gindulyte A, He J, He S, Li Q, Shoemaker BA, Thiessen PA, Yu B, Zaslavsky L, Zhang J & Bolton EE, PubChem 2019 update: improved access to chemical data. *Nucleic Acids Res*, 47 (2018) D1102.

30 Sterling T & Irwin JJ, ZINC 15 – Ligand Discovery for Everyone. *J Chem Inf Model*, 55 (2015) 2324.

31 Lovering F, Bikker J & Humblet C, Escape from flatland: Increasing saturation as an approach to improving clinical success. *J Med Chem*, 52 (2009) 6752.

32 Wei W, Cherukupalli S, Jing L, Liu X & Zhan P, Fsp3: A new parameter for drug-likeness. *Drug Discov Today*, 25 (2020) 1839.

33 Ertl P, Rohde B & Selzer P, Fast calculation of molecular polar surface area as a sum of fragment-based contributions and its application to the prediction of drug transport properties. *J Med Chem*, 43 (2000) 3714.

34 Daina A, Michielin O & Zoete V, ILOGP: A simple, robust, and efficient description of n-octanol/water partition coefficient for drug design using the GB/SA approach. *J Chem Inf Model*, 54 (2014) 3284.

35 XLOGP Program Version: 3.2.2.

36 Wildman SA & Crippen GM, Prediction of physicochemical parameters by atomic contributions. *J Chem Inf Comput Sci*, 39 (1999) 868.

37 Moriguchi I, Hirono S, Liu Q, Nakagome I & Matsushita Y, Simple Method of Calculating Octanol/Water Partition Coefficient. *Chem Pharm Bull (Tokyo)*, 40 (1992) 127.

38 Lipinski CA, Lombardo F, Dominy BW & Feeney PJ, Experimental and computational approaches to estimate solubility and permeability in drug discovery and development settings. *Adv Drug Deliv Rev*, 46 (2001) 3.

39 Moriguchi I, Hirono S, Nakagome I & Hirano H, Comparison of Reliability of log P Values for Drugs Calculated by Several Methods. *Chem Pharm Bull (Tokyo)*, 42 (1994) 976.

40 FILTER-IT Program Version: 1.0.2.

41 Delaney JS, ESOL: Estimating aqueous solubility directly from molecular structure. *J Chem Inf Comput Sci*, 44 (2004) 1000.

42 Ali J, Camilleri P, Brown MB, Hutt AJ & Kirton SB, *In silico* prediction of aqueous solubility using simple QSPR models: The importance of phenol and phenol-like moieties. *J Chem Inf Model*, 52 (2012) 2950.

43 Martin YC, A bioavailability score. *J Med Chem*, 48 (2005) 3164.

44 Baell JB & Holloway GA, New substructure filters for removal of pan assay interference compounds (PAINS) from screening libraries and for their exclusion in bioassays. *J Med Chem*, 53 (2010) 2719.

45 Brenk R, Schipani A, James D, Krasowski A, Gilbert IH, Frearson J & Wyatt PG, Lessons Learnt from Assembling Screening Libraries for Drug Discovery for Neglected Diseases. *ChemMedChem*, 3 (2008) 435.

46 Teague SJ, Davis AM, Leeson PD & Oprea T, The design of leadlike combinatorial libraries. *Angew Chem Int Ed Engl*, 38 (1999) 3743.